University of Pennsylvania
ScholarlyCommons

Departmental Papers (MEAM)

Department of Mechanical Engineering & Applied Mechanics

3-13-2021

Push-On Push-Off: A Compliant Bistable Gripper with Mechanical Sensing and Actuation

Jessica McWilliams
University of Pennsylvania, jmcw@seas.upenn.edu

Yifan Yuan
University of Pennsylvania

Jason Friedman
University of Pennsylvania

Cynthia Sung
University of Pennsylvania, crsung@seas.upenn.edu

Follow this and additional works at: https://repository.upenn.edu/meam_papers

Part of the Applied Mechanics Commons

Recommended Citation

McWilliams, Jessica; Yuan, Yifan; Friedman, Jason; and Sung, Cynthia, "Push-On Push-Off: A Compliant Bistable Gripper with Mechanical Sensing and Actuation" (2021). *Departmental Papers (MEAM)*. 307.
https://repository.upenn.edu/meam_papers/307

To see the bistable gripper grasping and releasing objects, check out the supplementary video:
https://www.youtube.com/watch?v=z50dYYzYvls

This paper is posted at ScholarlyCommons. https://repository.upenn.edu/meam_papers/307
For more information, please contact repository@pobox.upenn.edu.

Push-On Push-Off: A Compliant Bistable Gripper with Mechanical Sensing and Actuation

Abstract

Grasping is an essential task in robotic applications and is an open challenge due to the complexity and uncertainty of contact interactions. In order to achieve robust grasping, systems typically rely on precise actuators and reliable sensing in order to control the contact state. We propose an alternative design paradigm that leverages contact and a compliant bistable mechanism in order to achieve "sensing" and "actuation" purely mechanically. To grasp an object, the manipulator holding our end effector presses the bistable mechanism into the object until snap-through causes the gripper to enclose it. To release the object, the tips of the gripper are pushed against the ground, until rotation of the linkages causes snap-through in the other direction. This push-on push-off scheme reduces the complexity of the grasping task by allowing the manipulator to automatically achieve the correct grasping behavior as long as it can get the end effector to the correct location and apply sufficient force. We present our dynamic model for the bistable gripping mechanism, propose an optimized result, and demonstrate the functionality of the concept on a fabricated prototype. We discuss our stiffness tuning strategy for the 3D printed springs, and verify the snap-through behavior of the system using compression tests on an MTS machine.

Acknowledgements

Support for this project has been provided in part by NSF Grant No. 1138847 and DGE-1845298. We also thank Terry Kientz, Jeremy Wang, Peter Szczesniak, and Joe Valdez for their assistance with the fabrication, and Neal Tinaikar for assistance with initial prototypes. We are grateful.

Keywords

Grippers and Other End-Effectors, Compliant Joint/Mechanism, Additive Manufacturing

Disciplines

Applied Mechanics | Engineering | Mechanical Engineering

Comments

To see the bistable gripper grasping and releasing objects, check out the supplementary video:

https://www.youtube.com/watch?v=z50dYYzYvls

This conference paper is available at ScholarlyCommons: https://repository.upenn.edu/meam_papers/307

Push-On Push-Off: A Compliant Bistable Gripper with Mechanical Sensing and Actuation

Jessica McWilliams, Yifan Yuan, Jason Friedman, and Cynthia Sung

***Abstract*— Grasping is an essential task in robotic applications and is an open challenge due to the complexity and uncertainty of contact interactions. In order to achieve robust grasping, systems typically rely on precise actuators and reliable sensing in order to control the contact state. We propose an alternative design paradigm that leverages contact and a compliant bistable mechanism in order to achieve "sensing" and "actuation" purely mechanically. To grasp an object, the manipulator holding our end effector presses the bistable mechanism into the object until snap-through causes the gripper to enclose it. To release the object, the tips of the gripper are pushed against the ground, until rotation of the linkages causes snap-through in the other direction. This push-on push-off scheme reduces the complexity of the grasping task by allowing the manipulator to automatically achieve the correct grasping behavior as long as it can get the end effector to the correct location and apply sufficient force. We present our dynamic model for the bistable gripping mechanism, propose an optimized result, and demonstrate the functionality of the concept on a fabricated prototype. We discuss our stiffness tuning strategy for the 3D printed springs, and verify the snap-through behavior of the system using compression tests on an MTS machine.**

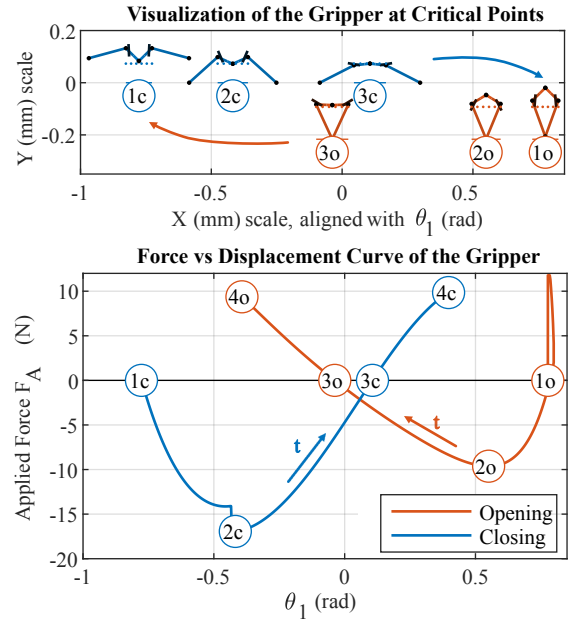

Fig. 1. [Top] Visualization showing a side view of the gripper at critical points. The solid and dashed horizontal lines indicate the the ground and object height for each case respectively, and the arrows indicate snap-through between states. [Bottom] Applied force versus θ_1 for both opening and closing procedures for the optimized version of the gripper, plotted after a median filter. In each case, the location of applied force y_A follows a constant velocity trajectory toward the ground. Arrows indicate the direction in which time advances for each curve. Critical points for the optimization include: the initial equilibrium configuration (1), applied force requirement (2), unstable equilibrium at which snap-through occurs (3), and maximum force (4). The discontinuities at (2c) and (1o) correspond to contact events between the tips and the ground. Due to geometric constraints from contact with the ground and object, each curve on this plot only shows one stable equilibrium; however, snap-through to the other state will occur as long as the force at (4) is positive.

I. INTRODUCTION

Grasping is a widely studied problem in robotics due to the prevalence of grasping tasks in everyday life. Robotic manipulators require the ability to pick up and release objects reliably despite differences in object size, weight, geometry, and material properties. A great deal of research has gone into gripper design, encompassing various materials and actuation strategies [1].

Traditional robotic grippers generally use pneumatic or electric actuation to apply large forces that tighten two rigid fingers about a particular object. However, these approaches often require complex perception and tactile feedback control, for example when manipulating cables [2], which often becomes too slow for real-time application and too expensive for practical and efficient fabrication [3]. Further challenges in rigid gripper control and design arise when compensating for variation in object shape and size, and subsequently applying forces with precise magnitudes that grasp without permanently damaging the object [4].

In response to these shortcomings, there has recently been a growing interest in minimally actuated grippers. While many existing hands have large numbers of degrees of freedom (DOF), it has been shown that in actuality, only a few actuated DOFs are necessary to perform a successful and robust grasp [5]. In certain cases the number of actuators and thus degree of underactuation has been varied while still achieving desired performance [6]. A recent zero-DOF example leverages the inertia of the object for passive dynamic grasping without any actuators, sensors, or moving parts in the end-effector [7].

Soft robotic grippers in particular have greatly advanced the field, by reducing the gripper weight [8], cost, and actuation requirements, as well as contributing high robustness and conformity to variance in object geometry [1], [9]. Examples such as [10], [11] demonstrate that a soft material

The authors are with the General Robotics, Automation, Sensing & Perception (GRASP) Lab at the University of Pennsylvania, Philadelphia, PA, USA. Emails: {jmcw, yuanyyf, jasonf27, crsung}@seas.upenn.edu. Support for this project has been provided in part by NSF Grant No. 1138847 and DGE-1845298. We also thank Terry Kientz, Jeremy Wang, Peter Szczesniak, and Joe Valdez for their assistance with the fabrication, and Neal Tinaikar for assistance with initial prototypes. We are grateful.

and vacuum pump are sufficient for a force closure grasp via particle jamming without any additional perception required. Bio-inspired soft gripper designs draw inspiration from the stiffness-variable multi-fingered human hand [12], [13], the wrap-around style of elephant trunks [1], the high friction overhead enclosure of starfish [14], and the layered beams of alternating material in Fin Rays [15].

In particular, bistability has been demonstrated to increase grasp forces and speeds while enabling passive grasping without actuators. Bistable grippers demonstrate grasping driven by storage of spring-like energy, using pneumatic actuation inspired by biological systems such as the Venus flytrap [16], or alternatively, passive grasping which facilitates actuation flexibility and strain energy tuning [17] and results in fast grasping speeds [18].

Similarly, mechanisms inspired by buckling beam theory [19], [20] and bistable origami mechanisms [21], [22], [23] have been able to demonstrate minimally actuated grasping of a wide array of objects. Despite the versatility of these grippers, however, ungrasping an object remains a challenge for them. As a result, for most robotic manipulators, binary actuation is required in the form of SMA [24], pneumatics [25], or magnets [26] to release the object.

We are inspired by mechanisms such as [27], [28], which provide push-on push-off switches, potentially opening the way for completely unactuated grasping and release of objects. Grippers using push-on push-off designs would reduce the amount of actuation, weight, and control needed for a gripper, enabling use in applications such as aerial vehicles, where minimizing weight has a large effect on vehicle performance [29].

We propose a novel grasping mechanism that achieves "sensing" and "actuation" by leveraging a compliant bistable mechanism. The bistable gripper does not require any electrical components, which will allow it to be easily mounted to various robotic systems. Furthermore, the external forces required for closing on the object and opening to release the object are similar. Both require the manipulator to push the gripper in the direction of the object. Changes in boundary conditions enable the same applied force to result in bidirectional state-switching, thus achieving a push-on push-off behavior.

The paper is organized as follows: Section II details the dynamic model of our gripper and outlines design parameters that affect its performance. Section III outlines our approach to optimizing the gripper design to maximize the versatility of the gripper and its ability to both grasp and release objects. Section IV describes our fabricated prototype, and Section V includes evaluations of its performance. Section VI concludes with discussion and directions for future work.

II. DYNAMIC MODELING

A. Bistable Gripper Design Overview

We examine a gripper, shown in Fig. 2, which is able to open and close by leveraging a bistable structure in place of traditional actuators. The gripper is symmetric about a vertical plane through its centerline, and each side contains a linear spring, two linkages, and a torsional spring. The parameters defining the design are listed in Table II. A ring of fixed radius $R < L_{0,0}$ forms the bistable structure by constraining the springs in opposition such that the springs have an equilibrium angle, $\theta_{1,0}$ relative to horizontal. The remaining components leverage the bistable mechanism to create a grasping behavior. The gripper requires only that an external force pushes it toward the object in order for it to close. To open, a force must be applied in the direction of the surface onto which we intend to release the object. During the opening procedure, the angle θ_2 must change to allow for snap-through to occur. Therefore, we connect Link 1 and Link 2 with a torsional spring rather than a fixed connection.

TABLE I
GRIPPER VARIABLES

Design Variables	[*= optimized, ** = function of other variables]
$L_{0,0}$	Resting length of linear spring
R	Radius of the ring**
L_1	Length of Link 1 (from A to B)*
L_2	Length of Link 2 (from B to C)**
$\theta_{1,0}$	Rest angle of Link 1*
$\theta_{2,0}$	Rest angle (of spring) between Links 1 and 2
$\theta_{2,m}$	Angle of mechanical stop activation*
k_1	Linear spring constant*
k_2	Torsional spring constant
p	A to E distance along Link 1, normalized by L_1*
d_x, d_y	Distance from A to D **
s	Distance from B to where F contacts Link 2
State Variables q	
θ_1	Angle of Link 1 from horizontal
θ_2	Angle between Links 1 and 2
y_A	Height of the ring above the ground

The central bistable structure has two stable equilibria at $\theta_{1,0}$ and $-\theta_{1,0}$ and one unstable equilibrium at $\theta_1 = 0$ (when the springs directly oppose each other). To switch between the two stable equilibria, a force must be applied at center O to compress the springs until they pass through the unstable equilibrium. Once θ_1 is past the unstable equilibrium, snap-through occurs and no external force is required for the rest of the transition. This is due to the springs' elastic potential energy, which will be released and cause the springs to go to the other equilibrium. In most uses of bistability, force would be applied at the same location but in the opposite direction to return to the first equilibrium.

In contrast, the gripper mechanism introduced in this paper uses linkages to give the bistable structure a push-on push-off behavior. A downward external force is applied to the ring at A both for closing and opening the gripper, but due to the geometry of the gripper and the changes in contact forces, the downward force causes the bi-directional switching behavior. Fig. 1 shows the force displacement curves for the gripper mechanism, with the force corresponding to the applied force F_A needed at time t in order to track a constant velocity downward trajectory for the ring. Visual representations of the gripper at the initial equilibrium configuration (1), required force (2), and unstable equilibrium (3) key points are also provided, as these are the critical points for designing the snap-through behavior.

During the closing procedure, the gripper begins in the equilibrium configuration visualized in Fig. 1 by (1c). The manipulator holding the gripper applies the necessary force F_A for point A (shown in Fig. 2) to track a trajectory of constant downward velocity. Once point O on the gripper contacts the object, θ_1 approaches zero from the negative side and the springs are compressed, so for motion to continue the the magnitude of F_A. At (2c), the magnitude of the applied force hits a maximum. This point tells us that in order to cause snap-through, the manipulator must be capable of applying a downward force of at least $F_{A,2c}$. The discontinuity near (2c) indicates that the tips of the gripper have touched the ground. Depending on the geometry of the gripper, this discontinuity may appear either to the left or the right of (2c). Further compression of the bistable mechanism leads us to the x-intercept (3c), which is the unstable equilibrium point. The instant that θ_1 is nudged to the other side of this point, snap-through will occur and reversing the trajectory of A will result in the gripper progressing to (1o), as indicated by arrows in the top plot of Fig. 1. If the manipulator continues to follow the downward trajectory it reaches (4c), at which point it becomes impossible to continue lowering A because the mechanical stop engages and prevents θ_2 from increasing any further. For some combinations of parameters, there is no unstable equilibrium and the force $F_{A,4c}$ is negative. This would indicate that the gripper cannot snap-through to pick up the object.

During the opening procedure, the gripper begins in the equilibrium configuration shown at (1o). Similarly to the closing procedure, the manipulator holding the gripper applies F_A to maintain a constant downward velocity. This time, the different initial configuration leads to boundary conditions which will cause opening. Once the tips of the gripper C contact the ground, θ_2 begins to decrease causing θ_1 to start moving toward zero, this time approaching from the positive side. At (2o) we reach the minimum of F_A, which gives us the required downward force to cause snap-through. At (3o), we reach the unstable equilibrium for opening. This will always occur with $\theta_{1,3o} < 0$ due to the resistance from the torsional spring. If displacement continues downward slightly, then snap-through will occur and reversing the motion of A will result in separation of the tips, releasing the object.

B. Equations of Motion

We use the Euler-Lagrange method to derive the dynamics of the system. The state variables $q = [\theta_1, \theta_2, y_A]$ are chosen to define the system, and we assume that the links are rectangular bodies with uniform mass distribution and point O is a point mass. The potential energy (Eq. (1)) and kinetic energy (Eq. (2)) are computed

$$\begin{aligned} V =& \frac{1}{2}k_1\left(L_0 - \frac{R}{cos(\theta_1)}\right)^2 + \frac{1}{2}k_2(\theta_2 - \theta_{2,0})^2 \\ &+ g(m_1y_1 + m_2y_2 + m_Ay_A + m_sy_s + m_0y_0) \end{aligned} \tag{1}$$

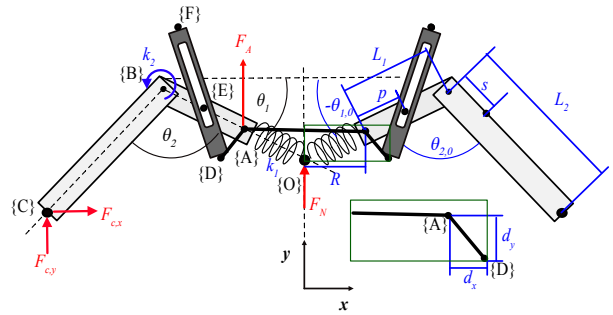

Fig. 2. Coordinate Frames for the symmetric bistable gripper in the open state. The darker grey represents the mechanical stop linkage, discussed in Section II-D. External forces are shown in red on the left half of the gripper, while design parameters are shown on the right half in blue. Points at A and D are fixed relative to one another on the ring (dark line)

$$\begin{aligned} T =& \frac{1}{2}m_1\dot{x_1}^2 + \frac{1}{2}I_1\dot{\theta_1}^2 + \frac{1}{2}m_2\dot{x_1}^2 + \frac{1}{2}I_2\dot{\theta_2}^2 && \text{Links} \\ &+ \frac{1}{2}m_A\dot{y_A}^2 + \frac{1}{2}m_0\dot{y_0}^2 && \text{Ring, } O \\ &+ \frac{1}{2}m_s\dot{y_A}^2 + \left(\frac{1}{2}I_s\omega_{MS}^2\right) && \text{Mech. Stop} \end{aligned} \tag{2}$$

and then the Euler-Lagrange formula is applied. The result is rearranged into the matrix form of the manipulator equations:

$$M\ddot{q} + C\dot{q} + N = J^T\lambda \tag{3}$$

C. Hybrid Dynamic Model

To obtain the constraint forces $\lambda = [F_{c,y}, F_{c,x}, F_A, F_N]^T$ on the right hand side of the manipulator equation (3), we assume that the sequence of contact events is known and develop gap functions ϕ to behave as guards for the hybrid dynamic system. When $\phi_i \neq 0$, the constraint should not be active and we will set its corresponding constraint force $\lambda_i = 0$ during the integration of the dynamics. When $\phi_i = 0$, the constraint is active and we may have a nonzero λ_i.

In the closing procedure, the gripper follows the contact sequence: O to object, C to ground, mechanical stop F to Link 2. For opening, the gripper just contacts the ground and then the ring continues descending. Each time a contact is added, we must activate a constraint at that contact to prevent penetration.

When there is contact with the ground, a kinematic loop is formed between points A, B, and C. We can check that the y-displacement when traversing the loops is zero, which we express as the following constraint equation:

$$\phi_1 = y_A - L_1\sin(\theta_1) - L_2\sin(\theta_2 - \theta_1) \tag{4}$$

Similarly, the x displacement should match the ring radius when the tips of the gripper touch each other in the closed state.

$$\phi_2 = R - L_1\cos(\theta_1) - L_2\cos(\theta_2 - \theta_1) \tag{5}$$

We track the downward trajectory $y_{A,des}$ with displacement control in our dynamic model to simulate the motion of

a manipulator. The manipulator will attach to the ring and directly control the position of A

$$\phi_3 = y_A - y_{A,des} \tag{6}$$

We also derive the distance between the mechanical stop and Link 2, but due to its complexity and minimal apparent effect we omit it. Finally, the contact with the object creates a trigonometric relationship between the ring height and the angle of the bistable mechanism.

$$\phi_4 = y_A + R\tan(\theta_1) - H_{obj} \tag{7}$$

Following the procedure laid out in [30], we take the Jacobian of each constraint with respect to the chosen minimal coordinates $q = [\theta_1, \theta_2, y_A]^T$ and stack them vertically to obtain $J = \partial\phi/\partial q$ in Eq. (3). Finally, we use the Baumgarte stabilization technique to analytically approximate the constraint forces using

$$\lambda = -(JM^{-1}J^T)^+(JM^{-1}\tau + (\dot{J} + 2\alpha J)\dot{q} + \alpha^2\phi) \tag{8}$$

where $^+$ indicates the Moore-Penrose pseudo-inverse of a matrix. We choose the regularization parameter α to be 1,000 for all constraints, except for the ground penetration constraint which we set to 10,000. Note that since our system does not have actuators, $\tau = 0$. The use of Baumgarte stabilization technique allows us to solve what would be a differential algebraic equation as an ordinary differential equation, which we solve using MATLAB's ode45 with events to handle the addition and removal of constraints.

D. Mechanical Stop

Initial analysis of the gripper mechanism revealed that with a fixed angle mechanical stop, it is geometrically infeasible to find a straight-linked gripper which can fully enclose a cubic or spherical object that is sufficiently large to cause snap-through. This is because snap-through in each direction requires the ring to be displaced until $y_A(t) \leq y_{crit}$. When closing, contact with the ground at C of Link 2 places a lower bound on $y_A(t)$, which implies that an object must be sufficiently tall H_{min} to cause snap-through. Since O moves inside the gripper while opening, there is a maximum height object H_{max} which can be enclosed. Our analysis showed that for a closure grasp of a spherical object, $H_{min} > H_{max}$ and there is no feasible object height when there is a fixed mechanical stop.

To reduce H_{min} such that $H_{min} \leq H_{max}$, we designed a mechanical stop which will only constrain θ_2 when the gripper is closed. Inspired by [31], we first focused on the functionality of the bistable mechanism and then iterated over how to add the mechanical stop in a way that enhances the system's performance. We designed a moving mechanical stop that is inspired by an angle doubling drive. It consists of a driving link and a slotted link as shown in Fig. 2. The driving link in our system (Link 1) rotates about A, which is fixed to the ring, and has a peg located at E, which is p away from A. The slotted link is our mechanical stop, and it is constrained to rotate about D on the ring, which is offset from A by (d_x, d_y). The slot on the mechanical stop is constrained to the peg at E. The result is that the slotted mechanical stop exhibits a larger angular displacement than the driving link, as seen in Fig. 1 and Fig. 3. While the mechanical stop operates in a plane offset from that of Link 1, point F is extruded to allow the mechanical stop to contact Link 2. Thus, the mechanical stop engages and constrains θ_2 when the gripper is closed, but it rotates far away from Link 2 when the gripper is open so that y_A can get low enough to pick up smaller objects.

The mechanical stop design requires the placement of three colinear points: E on Link 1, D on the ring, and F on the mechanical stop which defines the length of the mechanical stop L_{ms}. Due to fabrication constraints, we require that when the mechanical stop is engaged, F contacts Link 2 at a distance of $s = 25$ mm away from joint B. The corresponding optimization parameter is $\theta_{2,m}$, the angle of the second link when the mechanical stop is engaged.

Optimization parameter p expresses the distance of E from A normalized by L_1, and determines the point along which the mechanical stop slides. Finally, the point of rotation for the stop is computed using the co-linearity of the three points. For fabricability, we require that the position of D is at least 14 mm away from A to prevent interference between the fasteners. If it is too close, we move E away from A incrementally until a feasible solution is found or deemed non-existent.

III. Optimization

A. Grid Search Across Parameters

We select an optimal gripper using a grid search. Due to the high dimensionality of the design space, we first run Principal Component Analysis (PCA) on a smaller, sparsely-discretized dataset to determine which variables have the greatest effect on the critical points from the simulation marked in Fig. 1. The PCA determined that we should focus our grid search to have the highest resolution on L_1 and $\theta_{1,0}$. We optimize over the parameters $k_1, L_1, \theta_{1,0}, \theta_{2,m}$, and p described in Table I. Resting length $L_{0,0}$ is fixed to prevent arbitrary scaling of the gripper and s is fixed due to fabrication constraints. The remaining dimensions are uniquely determined by the other variables. Radius $R = L_{0,0}\cos(\theta_{1,0})$ by definition. We constrain the tips at C to meet when the gripper is closed without causing deformation of the bistable mechanism using the following relationship:

$$L_2 = (L_1 + L_{0,0}\cos(\theta_{1,0}))/\cos(\theta_{2,m} - \theta_{1,0}) \tag{9}$$

The mechanical stop's parameters d_x, d_y, and L_{ms} are computed via trigonometric relations.

For each gripper design trial, we first perform a compression simulation of the opening procedure and compute the maximum object size H_{max}, assuming a spherical object. At the point of snap-through (3o), we compute the maximum inscribed circle that can fit between the triangle described by the tip of the gripper C and a horizontal line drawn through the center O. Next, we use this value as the height of the object in the closing gripper simulation. Before computing the critical points shown in Fig. 1, we use a median filter

of width 100 on the force data from the simulation, to ensure non-smoothness at contact events will not prevent the program from choosing the correct extrema.

After simulating 68,820 grippers, we eliminate grippers which do not exhibit bidirectional snap-through by only keeping grippers whose maximum force value (4c, 4o) on each curve is positive. This ensures that there exists some object that the gripper can successfully grasp and release, as mentioned in Section II-D. Due to our lightweight 3D printed links, we also constrain the magnitude of the required force for snap-through (2c, 2o) to be less than 20N to avoid breaking or bending the rigid links. There are also implicit requirements regarding the torsional spring stiffness: it must be stiff enough to counteract the effect of gravity on Link 2 when the gripper is open, yet it must not be so stiff that it prevents snap-through during the opening procedure. We estimated that the off-the-shelf torsional spring with stiffness 0.0016 N/rad is sufficient to support the mass of our second link with minimal deformation, while still remaining easily compressible. Grippers which exhibit bidirectional snap-through with this spring automatically satisfy these constraints.

B. Objective

Many of the high stiffness candidates exceeded the actuation force constraint, and many of the low stiffness designs were infeasible, likely due to the ratio of k_1 with k_2. From the remaining 36,205 valid design candidates, we desire a gripper that is able to tolerate variation in objects. The maximum sized object which fits inside H_{max} is already geometrically determined from the opening simulation. The force displacement curve for the closing gripper varies with object height since the gripper makes contact with both the object and the ground. We notice that decreasing H_{obj} shifts the x-intercept to the right, as shown by the Closing Sim curves in Fig. 5 and Fig. 6. As a notion of ease of snap-through, we aim to minimize the rotation of the bistable mechanism which is necessary for snap-through. Thus, we desire the gripper's unstable equilibria angles ($\theta_{1,3c}$, $\theta_{1,3o}$) to be as close to their respective initial configurations ($\theta_{1,1c}$, $\theta_{1,1o}$) as possible. Note that this means we need to negate $\theta_{1,3o}$ in our objective since θ_1 proceeds from positive to negative as the gripper opens. Similarly, we want to make sure that the maximum force on the closing curve remains positive for objects of decreased size, so we seek to increase the maximum force on the closing curve ($F_{A,4c}$).

Since the same robot closes and opens the gripper, we incorporate the normalized difference between the force required for snap-through on each curve ($F_{A,2c}$, $F_{A,2o}$) as a symmetry objective. For consistency, we normalize all forces in the objective by F_{2o}. Finally, we desire to limit material consumption in building our gripper. We consider the material efficiency to be the radius of the largest inscribed circle ($0.5H_{max}$) divided by the lengths of the main linkages. The final objective f is a sum of the aforementioned objectives:

$$f = \theta_{1,3c} - \theta_{1,3o} + \frac{F_{A,4c}}{F_{A,2o}} + \frac{F_{A,2o} - F_{A,2c}}{F_{A,2o}} + \frac{0.5H_{max}}{L_1 + L_2} \quad (10)$$

TABLE II
FABRICATED GRIPPER PARAMETERS

Parameter	Sample Space	Handpicked	Optimized
k_1 (N/mm)	2, 5, 10	5	5
k_2 (N/rad)	0.0016	0.0016	0.0016
$L_{0,0}$ (mm)	30	30	30
L_1 (mm)	28 : 2 : 100	50	40
L_2 (mm)	-	170	147
$\theta_{1,0}$ (deg)	30 : 0.5 : 45	40	44.5
$\theta_{2,m}$ (rad)	1.7 : 0.1 : 2.0	1.9	2
p (mm/mm)	0.4 : 0.05 : 0.6	0.55	0.6
L_{ms} (mm)	-	59	48
R (mm)	-	22.9	21.4
d_x (mm)	-	20	16
d_y (mm)	-	6.0	3.9

We select the set of parameters that minimizes f. The optimal parameters are shown in Table II.

IV. FABRICATION

A. Prototype

The fabricated prototype based on our design and analysis is shown in Fig. 3, with relevant components labeled. All of the components are 3D printed on either a MakerBot Replicator 2 (MakerBot Industries, LLC) or a MakerGear M3-ID (MakerGear LLC). The linkages, mechanical stop, and hooks are printed with PLA filament of 0.75 mm diameter (MakerGear LLC) and the linear spring is printed by flexible transparent Thermoplastic Polyurethane (TPU) filament (Tronxy). Components are connected at joints by 5.8 mm diameter binding barrels (McMaster-Carr 93121A345) and the torsional spring is 120 Degree Angle, Left-Hand Wound, 0.380" OD (McMaster-Carr 9271K355).

The ring is printed as two pieces placed on the front and back with handles for mounting. Link 1 and Link 2 are also printed in two halves and snapped together. The linear spring is located at the center of the gripper. It contains two equal TPU printed springs connected with an axle. The detailed design of the linear spring is discussed in Section IV-B. Block extrusions on Link 1 and the spring constrain them to be colinear. The mechanical stops surround Link 1 and Link 2 with an axle corresponding to F which contacts Link 2 to prevent the hooks from opening while holding an object.

B. Linear Spring Design

We construct our linear spring by 3D printing with the soft material of TPU, which displays high flexibility and elasticity [32]. Unlike hard 3D printing filaments (PLA, ABS, etc.) [33], the TPU material can exhibit a large range of stiffness in its printed products, as shown in Fig. 4. Thus, the 3D printed TPU products allow us to customize both the stiffness and geometry of the spring by tuning the infill parameters. Our design is based on the general dog-bone sample for tensile/compression tests, which contains two blocks for connections and the diamond (square) pattern in the middle. As shown in Fig. 3, the cell size and wall thickness parameterize the structure and the infill percentage of the diamond pattern.

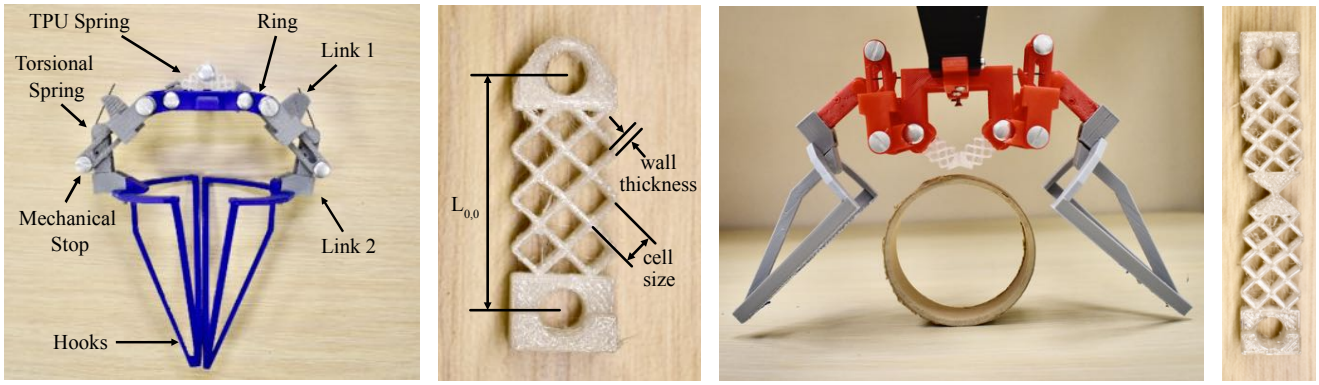

Fig. 3. [Left] The label diagram of the handpicked gripper while closed. [Middle] The TPU spring with stiffness of 5 N/mm. The holes on each end fasten the spring to the ring. The diamond pattern has the cell size of 4.5 mm, wall thickness of 0.56 mm. [Right] An image of the optimized gripper while open. [Far Right] The alternate spring design which reduces in-plane bending of the TPU pattern and eliminates out-of-plane bending.

We perform compression tests in order to determine the stiffness of the spring. During the tests, the material itself will not be compressed until the vacancy squares have been completely compressed, so the stiffness of the spring is much less than that of solid TPU. When designing the spring, closed-shaped squares are required for preventing the self-collision of incomplete squares. To resist buckling, we position the diamond pattern such that the spring contains three columns.

We use the compression tests from the MTS machine to determine the mechanical properties of the the linear springs. We tested different infill percentages created by changing wall thickness of each of the diamond cells. Fig. 4 shows the resulting force-displacement curves for the different infill percentage samples. The curves are fairly linear in the low strain (<10%) region, which is the relevant region for the bistable gripper. Therefore, we determine the parameters to achieve spring stiffness k using the formula $k = \frac{EA}{L}$ where E is the Elastic modulus, A is the cross-sectional area, and L is the length of the spring. For cell sizes of 4.5 mm, the spring has a cross-section of 7.6 mm $\times$ 12.7 mm and length 21 mm. The elastic modulus of a spring having stiffness of 5 N/mm should be 1.085 MPa. Using our test results, we find that a cell size of 4.5 mm and wall thickness of 0.75 mm gives an infill percentage of 30.56%. This results in an elastic modulus of 0.7843 MPa corresponding to stiffness of 4.86 N/mm, which decide is close enough for the purposes of checking prototype functionality.

V. EVALUATION

We fabricate two prototypes for comparison: a gripper that used manually tuned parameters designed by a human engineer, and the gripper resulting from the optimization. We verify the functionality of the handpicked prototype by testing it on a sphere with diameter 84 mm, which is near to its predicted maximum size sphere. The gripper successfully grasps and releases the object (see video). For the optimized gripper, we demonstrate the successful grasping and releasing of three different objects.

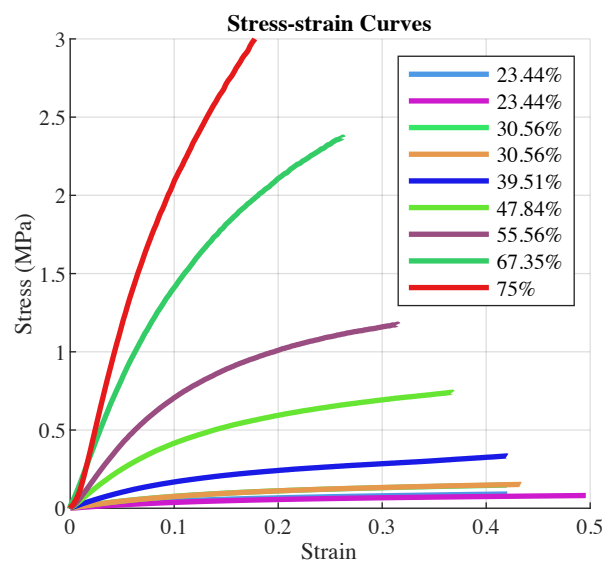

Fig. 4. The Strain-Stress curves of different infill percentages by the different combinations of cell size and wall thickness. X axis- Strain of the top surface; Y axis: Stress applied on the top surface. Repeated percentages indicate different design parameters to achieve the same infill percentage. The data shows that the infill percentage is the dominating factor.

We compare the two grippers in simulation and predict that the handpicked gripper can pick up objects ranging in height from 45 mm to 84 mm, while the optimized gripper can pick up objects with heights of 25 mm to 74 mm, indicating that the range of graspable objects is larger with the optimized gripper. The optimized gripper successfully picked up an object which was 35 mm tall during testing. However, an object that is 35 mm tall is sufficient to cause snap-through in the handpicked prototype also, even though it did not result in a successful grasp. This is because the TPU springs bend easily (as seen in the video of our MTS tests). Since θ_1 ultimately controls the angle of the mechanical stop, the mechanical stop often fails to constrain θ_2. A negative consequence of this is that only light objects can be successfully grasped by the current prototypes and not

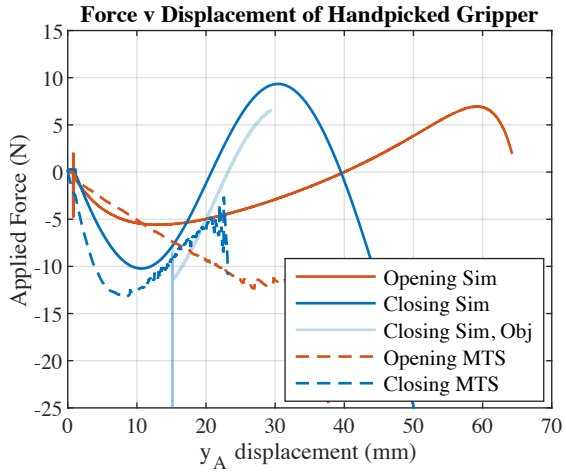

Fig. 5. The comparison of the MTS tests versus the simulation for the handpicked gripper. Since the MTS moves downward continuously, after the point of snap-though compression of rigid material begins. The lack of agreement between the opening curves is largely due to bending in the TPU springs. The maximum size graspable object H_{max} is determined during the Opening Sim. We include closing simulations with an object of height H_{max} (Closing Sim, Obj) and with a very tall object (Closing Sim) to show the effect that reducing the object height has on the snap-through behavior while closing. Smaller objects are harder to grasp because contact of Link 2 with the ground requires deformation of the torsional spring.

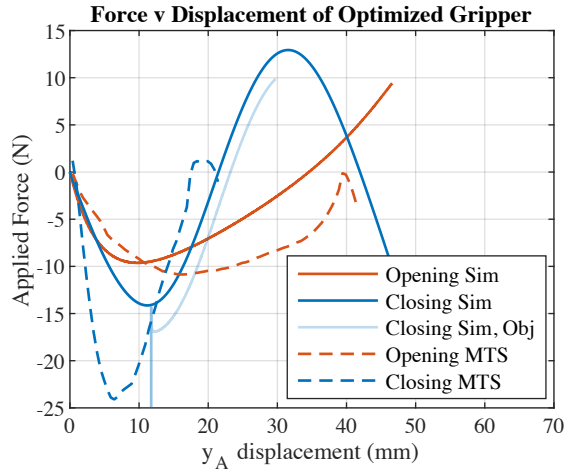

Fig. 6. The comparison of the MTS tests versus the simulation for the optimized gripper. During this trial, we used an alternative spring design that prints the bistable mechanism out of one piece using a thin segment between the two halves instead of the axle. We found that the bending of springs in the bistable mechanism is reduced, resulting in better agreement with the simulation in the opening curve, as compared with the bistable mechanism manufacturing method in Fig. 5.

every instance of snap-through results in a successful grasp. However, during the closing procedure, the springs can bend even when the mechanical stop should be preventing the system from compressing further, so smaller objects than predicted can cause snap-through and potentially be grasped.

We compare the simulation model with the prototypes quantitatively by performing compression tests on an MTS machine. We use a custom fixture to hold the ring on the crosshead and a standard compression platen on the bottom. We perform the opening tests without an object to replicate the simulation condition. The compression test results for the handpicked and optimized parameters are shown in Fig. 5 and Fig. 6 respectively.

The handpicked and optimized grippers' force displacement curves match fairly well for the closing curve with some apparent offset in the stiffness which could result from variation in the spring stiffness or additional friction in the mechanism. For the opening curves, the un-modeled bending of the TPU springs during the opening transition leads to a change in the force displacement curve. This is especially apparent from the handpicked gripper data in Fig. 5. We found that 3D printing the two springs as one piece and replacing the axle at O with a thin region of TPU, as shown in Fig. 3 prevents out-of-plane bending and reduces the effect of the in-plane bending of the linear springs. The MTS data for the optimized gripper in Fig. 6 was taken with this redesigned version of the spring, and the agreement of the opening curves and the simulation is stronger. Our video of the test indicates less in-plane bending within the spring pattern, which we attribute to the reduction of friction at the joint O. However, the TPU hinge also behaves as a torsional spring and changes the contact with the object when closing, which we expect accounts for much of the increase in stiffness of the mechanism.

We also demonstrate the gripper's ability to act as a perching mechanism in our supplementary video. Perching typically requires much coordination between the actuation and sensing in order to achieve a highly dynamic and contact sensitive motion. In contrast, our concept automatically closes when it contacts an object with sufficient force.

VI. CONCLUSION

We have demonstrated a novel bistable gripping mechanism that exhibits a push-on push-off behavior for grasping and releasing objects. The gripper leverages a compliant mechanism to achieve grasping without requiring any actuators or sensors. We simulated the gripper and demonstrated that the fabricated results exhibit similar snap-through characteristics to the simulation. We experimentally validated that the gripper is able to grasp and release objects. We also suggest the potential usefulness of this mechanism for perching or other highly dynamic applications.

Future work will perform a more thorough optimization procedure and seek to better understand how to leverage the compliant components of the design. A dataset with finer discretization and greater range in spring stiffnesses will allow for deeper exploration of the relationship between k_1 and k_2. For greater efficiency, we plan to switch to a gradient based optimization method since our objective is smooth.

While the snap-through behavior of the gripper is reliable, its robustness in grasping objects is currently limited because our simulation neglects object mass. We plan to remove the constraint that Link 2 is geometrically determined from the other variables (Eq. 9) to allow it to be oversized, which we hypothesize will lead to an increase in grasp force and

allow for more reliable grasping of objects. By adding the contact force at the tips to the objective, we can explore optimization for other modes of grasping, such as pinching. The current prototype's hook geometry has also not been optimized in any way, and we plan to consider alternative designs to improve the reliability of the grasp and ensure the geometry of the hooks matches the mode of grasp which is desired. We also plan to extend the design to actualize the perching application.

We find that the TPU springs are prone to buckling, which prevents transmission of the angle from the bistable mechanism to the mechanical stop. Consequently, this prevents the gripper from lifting heavy objects and limits the reliability of the grasping behavior. 3D printing the bistable mechanism in one piece rather than two has already given some improvements in the angle transmission. In the future, we plan to replace our simulation's linear spring model with a beam bending model and investigate ways to mitigate or even leverage this behavior of the TPU springs in future prototypes.

References

[1] J. Shintake, V. Cacucciolo, D. Floreano, and H. Shea, "Soft robotic grippers," *Advanced Materials*, vol. 30, no. 29, p. 1707035, 2018.

[2] Y. She, S. Wang, S. Dong, N. Sunil, A. Rodriguez, and E. Adelson, "Cable manipulation with a tactile-reactive gripper," *arXiv preprint arXiv:1910.02860*, 2019.

[3] A. Zaki, A. Soliman, O. Mahgoub, and A. El-Shafei, "Design and implementation of efficient intelligent robotic gripper," in *International Conference on Modelling, Identification and Control*, 2010, pp. 710–716.

[4] W. Townsend, "The BarrettHand grasper–programmably flexible part handling and assembly," *Industrial Robot: An International Journal*, 2000.

[5] M. T. Mason, A. Rodriguez, S. S. Srinivasa, and A. S. Vazquez, "Autonomous manipulation with a general-purpose simple hand," *International Journal of Robotics Research*, vol. 31, no. 5, pp. 688–703, 2012.

[6] A. M. Dollar and R. D. Howe, "Joint coupling design of underactuated hands for unstructured environments," *The International Journal of Robotics Research*, vol. 30, no. 9, pp. 1157–1169, 2011.

[7] C. Mucchiani and M. Yim, "Dynamic grasping for object picking using passive zero-DOF end effectors," *IEEE Robotics and Automation Letters*, 2021.

[8] B. Mosadegh, P. Polygerinos, C. Keplinger, S. Wennstedt, R. F. Shepherd, U. Gupta, J. Shim, K. Bertoldi, C. J. Walsh, and G. M. Whitesides, "Pneumatic networks for soft robotics that actuate rapidly," *Advanced Functional Materials*, vol. 24, no. 15, pp. 2163–2170, 2014.

[9] J. Hughes, U. Culha, F. Giardina, F. Guenther, A. Rosendo, and F. Iida, "Soft manipulators and grippers: a review," *Frontiers in Robotics and AI*, vol. 3, p. 69, 2016.

[10] E. Brown, N. Rodenberg, J. Amend, A. Mozeika, E. Steltz, M. R. Zakin, H. Lipson, and H. M. Jaeger, "Universal robotic gripper based on the jamming of granular material," *Proceedings of the National Academy of Sciences*, vol. 107, no. 44, pp. 18 809–18 814, 2010.

[11] Y. Wei, Y. Chen, T. Ren, Q. Chen, C. Yan, Y. Yang, and Y. Li, "A novel, variable stiffness robotic gripper based on integrated soft actuating and particle jamming," *Soft Robotics*, vol. 3, no. 3, pp. 134–143, 2016.

[12] Y. Yang, Y. Chen, Y. Li, M. Z. Chen, and Y. Wei, "Bioinspired robotic fingers based on pneumatic actuator and 3D printing of smart material," *Soft Robotics*, vol. 4, no. 2, pp. 147–162, 2017.

[13] Z. Xu and E. Todorov, "Design of a highly biomimetic anthropomorphic robotic hand towards artificial limb regeneration," in *IEEE International Conference on Robotics and Automation (ICRA)*, 2016, pp. 3485–3492.

[14] F. Ilievski, A. D. Mazzeo, R. F. Shepherd, X. Chen, and G. M. Whitesides, "Soft robotics for chemists," *Angewandte Chemie*, vol. 123, no. 8, pp. 1930–1935, 2011.

[15] W. Crooks, G. Vukasin, M. O'Sullivan, W. Messner, and C. Rogers, "Fin ray® effect inspired soft robotic gripper: From the robosoft grand challenge toward optimization," *Frontiers in Robotics and AI*, vol. 3, p. 70, 2016.

[16] X. Wang, A. Khara, and C. Chen, "A soft pneumatic bistable reinforced actuator bioinspired by venus flytrap with enhanced grasping capability," *Bioinspiration & Biomimetics*, vol. 15, no. 5, p. 056017, 2020.

[17] T. G. Thuruthel, S. H. Abidi, M. Cianchetti, C. Laschi, and E. Falotico, "A bistable soft gripper with mechanically embedded sensing and actuation for fast closed-loop grasping," *arXiv preprint arXiv:1902.04896*, 2019.

[18] A. McLaren, Z. Fitzgerald, G. Gao, and M. Liarokapis, "A passive closing, tendon driven, adaptive robot hand for ultra-fast, aerial grasping and perching," in *IEEE/RSJ International Conference on Intelligent Robots and Systems (IROS)*, 2019, pp. 5602–5607.

[19] T.-A. Nguyen and D.-A. Wang, "A gripper based on a compliant bistable mechanism for gripping and active release of objects," in *International Conference on Manipulation, Automation and Robotics at Small Scales (MARSS)*, 2016.

[20] H. Zhang, J. Sun, and J. Zhao, "Compliant bistable gripper for aerial perching and grasping," in *International Conference on Robotics and Automation (ICRA)*, 2019, pp. 1248–1253.

[21] S. Rojas, D. M. Boston, and A. F. Arrieta, "Actuation simplification for grippers based on bioinspired spring origami," in *Bioinspiration, Biomimetics, and Bioreplication IX*, vol. 10965, 2019, p. 109650O.

[22] F. Zuliani, C. Liu, J. Paik, and S. M. Felton, "Minimally actuated transformation of origami machines," *IEEE Robotics and Automation Letters*, vol. 3, no. 3, pp. 1426–1433, 2018.

[23] H. Yasuda, K. Johnson, V. Arroyos, K. Yamaguchi, J. R. Raney, and J. Yang, "Leaf-like origami with bistability for self-adaptive grasping motions," *arXiv preprint arXiv:2011.01428*, 2020.

[24] S.-W. Kim, J.-S. Koh, J.-G. Lee, J. Ryu, M. Cho, and K.-J. Cho, "Flytrap-inspired robot using structurally integrated actuation based on bistability and a developable surface," *Bioinspiration & Biomimetics*, vol. 9, no. 3, p. 036004, 2014.

[25] R. Jitosho, K. Choi, A. Foris, and A. Mazumdar, "Exploiting bistability for high force density reflexive gripping," in *International Conference on Robotics and Automation (ICRA)*, 2019, pp. 1241–1247.

[26] Z. Zhang, X. Li, X. Yu, H. Chai, Y. Li, H. Wu, and S. Jiang, "Magnetic actuation bionic robotic gripper with bistable morphing structure," *Composite Structures*, vol. 229, p. 111422, 2019.

[27] H.-W. Huang and Y.-J. Yang, "A MEMS bistable device with push-on–push-off capability," *Journal of Microelectromechanical Systems*, vol. 22, no. 1, pp. 7–9, 2012.

[28] H.-W. Huang, F.-W. Lee, and Y.-J. J. Yang, "Design criteria for a push-on push-off MEMS bistable device," *Journal of Microelectromechanical Systems*, vol. 25, no. 5, pp. 900–908, 2016.

[29] M. Bugday and M. Karali, "Design optimization of industrial robot arm to minimize redundant weight," *Engineering Science and Technology, an International Journal*, vol. 22, no. 1, pp. 346–352, 2019.

[30] R. Tedrake, "Underactuated robotics: Algorithms for walking, running, swimming, flying, and manipulation (course notes for mit 6.832)," 2009. [Online]. Available: http://underactuated.mit.edu/

[31] J.-S. b. Plante, M. Santer, S. Dubowsky, and S. Pellegrino, "Compliant bistable dielectric elastomer actuators for binary mechatronic systems," in *International Design Engineering Technical Conferences and Computers and Information in Engineering Conference*, vol. 47446, 2005, pp. 121–126.

[32] H. Lee, R.-i. Eom, and Y. Lee, "Evaluation of the mechanical properties of porous thermoplastic polyurethane obtained by 3D printing for protective gear," *Advances in Materials Science and Engineering*, vol. 2019, p. 5838361, 2019.

[33] "Dimensional considerations on the mechanical properties of 3D printed polymer parts," *Polymer Testing*, vol. 90, p. 106656, 2020.